Novel and Highly Sensitive Electrochemical Sensor for the Determination of Oxytetracycline Based on Fluorine-Doped Activated Carbon and Hydrophobic Deep Eutectic Solvents

Narumon Wannasri, Pikaned Uppachai, Kompichit Seehamart, Sakwiboon Jantrasee, Nuttaya Butwong, Kanit Mukdasai, Illyas Md Isa, and Siriboon Mukdasai*

Read Online

ACCESS | ‖ Metrics & More | 📖 Article Recommendations | ⓢ Supporting Information

ABSTRACT: Residues of oxytetracycline (OTC), a veterinary antibiotic and growth promoter, can be present in animal-derived foods; their consumption is harmful to human health and their presence must therefore be detected and regulated. However, the maximum residue limit is low, and consequently highly sensitive and accurate detectors are required to detect the residues. In this study, a novel highly sensitive electrochemical sensor for the detection of OTC was developed using a screen-printed electrode modified with fluorine-doped activated carbon (F-AC/SPE) combined with a novel deep eutectic solvent (DES). The modification of activated carbon by doping with fluorine atoms (F-AC) enhanced the adsorption and electrical activity of the activated carbon. The novel hydrophobic DES was prepared from tetrabutylammonium bromide (TBABr) and a fatty acid (malonic acid) using a green synthesis method. The addition of the DES increased the electrochemical response of F-AC for OTC detection; furthermore, it induced preconcentration of OTC, which increased its detectability. The electrostatic interactions between DES and OTC as well as the adsorption of OTC on the surface of the modified electrode through H-bonding and $\pi-\pi$ interactions helped in OTC detection, which was quantified based on the decrease in the anodic peak potential (E_{pa} = 0.3 V) of AC. The electrochemical behavior of the modified electrode was investigated by cyclic voltammetry, differential pulse voltammetry, and electrochemical impedance spectroscopy. Under optimum conditions, the calibration plot of OTC exhibited a linear response in the range 5−1500 μg L^{-1}, with a detection limit of 1.74 μg L^{-1}. The fabricated electrochemical sensor was successfully applied to determine the OTC in shrimp pond and shrimp samples with recoveries of 83.8−100.5% and 93.3−104.5%, respectively. In addition to the high sensitivity of OTC detection, the proposed electrochemical sensor is simple, cost-effective, and environmentally friendly.
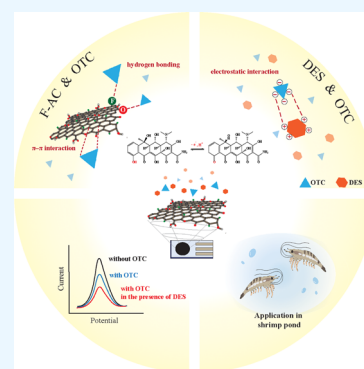
1. INTRODUCTION

Oxytetracycline (OTC) is an antibiotic in the tetracycline group that has been widely used in fields such as veterinary antibiotics and as animal growth promoters for the prevention and treatment of livestock diseases.[1,2] Residues of OTC can therefore be found in animal-derived foods; however, consumption of excessive residual antibiotics can seriously threaten human health.[3] Therefore, regulatory organizations such as the Food and Agriculture Organization (FAO), Food and Drug Authority (FDA), and Environmental Protection Agency (EPA) have set a maximum residue limit (MRL) of 0.2−1.2 mg L^{-1} for OTC in animal-derived foods.[4] As the MRL of OTC is low, sensitive detection techniques are required.

Several analytical techniques have been applied to detect OTC; accurate qualitative and quantitative results can be achieved by chromatographic methods.[5,6] Recently, electrochemical sensors have gained considerable attention owing to their high sensitivity and selectivity, fast analysis, rapid process, and low cost.[7] In recent years, there has been great development of new materials for electrochemical applications

such as carbon nanomaterials[8−10] and metal nanoparticles.[11−13] The attractiveness of nanomaterials including a unique characteristic, high chemical reactivity, and high surface area[14,15] significantly increases the sensitivity of electrochemical measures.[16] The attractive characteristic of the material can allow its use in the development of modified electrodes for the determination of target analytes with environmental concerns.

The modification of electrodes with nanomaterials has attracted attention, especially, carbon nanomaterials. Activated carbon (AC) is produced from environmental wastes with a high carbon content. AC is a low-cost material with distinguishable properties like a high specific surface area,

high porosity, and desired surface functionalization available for adsorption or chemical reactions.[17] In our previous study,[18] we synthesized AC from waste coffee grounds and modified AC with CuO-NPs for the detection of methyl parathion in soil samples. However, modification of AC is required to enhance its conductivity: doping of carbon nanomaterials can induce changes in their structure and properties that are favorable for catalytic applications. Thus, doping of AC is one approach to improve its electrical conductivity for enhanced detection of OTC.

Heteroatom-doped carbon materials have attracted particular attention because of their low cost and superior electrochemical properties, conductivity, and chemical stability.[19,20] Typically, heteroatom-doped carbon catalysts have been fabricated using nitrogen,[21,22] boron,[22–24] and phosphorus[22,25,26] as the doping elements and through post-treatment methods at high temperatures. A new class of halogen-doped carbon materials (i.e., fluorine,[27] chlorine,[28] bromine,[29] and iodine[30]) has, however, emerged as a promising choice for the efficient modification of carbon materials. Moreover, the surface area and electrical double-layer capacitance of carbon materials can be improved for use in supercapacitors by doping them with halogen atoms via a simple and effective method.[31,32] Among halogen-doped carbon materials, fluorine-doped carbon materials exhibit a highly efficient approach to increase the electrical conductivity: fluorine atoms enhance polarization owing to the presence of highly electronegative fluorine functional groups and refinement of pore structures/surfaces.[33] Therefore, fabricating fluorine-doped carbon with a high fluorine content, intact carbon structure, and superior electrochemical performance using a facile synthesis approach is critical.

Deep eutectic solvents (DESs) are eutectic mixtures comprising hydrogen bond donors and acceptors.[34,35] The interactions between these components lower the melting point of the mixture to below those of the individual components, leading to a liquid phase at room temperature. DESs are easy to prepare and offer several advantages[34,35] such as solubility of various organic and inorganic species, high biodegradability, low toxicity, and low cost. Among the different types of DESs, hydrophobic DESs have received considerable attention in recent years. However, to date, only a few hydrophobic DESs have been reported. Hydrophobic DESs are based on poorly water-soluble components such as tetraalkylammonium salts,[36] long-chain carboxylic acids,[37] menthol,[38] and lidocaine.[39] Ruggeria et al. studied the chemical and electrochemical properties of a hydrophobic DES that was prepared by mixing tetrabutylammonium chloride and decanoic acid.[40] Its hydrophobic nature was mostly extracted with aqueous media, such as volatile fatty acids[36] and pesticides.[41] The addition of a small amount of water to the hydrophobic DES not only can dramatically improve its electrical conductivity, but it can also improve the viscosity to a value suitable for electrochemical analysis. DESs are particularly appealing green systems for application in electrochemistry, such as in sensing and electrodeposition.[40] For example, hydrophobic DESs can induce preconcentration of compounds to be detected during electrochemical sensing, which is highly advantageous when the amount of compounds to be detected is very low. Hence, it is challenging to synthesize a novel DES to increase the performance of electrochemical sensors.

In this study, a novel and highly sensitive electrochemical sensor using a fluorine-doped activated carbon (F-AC)-modified screen-printed electrode (SPE) was fabricated for OTC detection. DES was used to induce the preconcentration of the target analyte to improve OTC detection. This is the first report on the use of a hydrophobic DES composed of tetrabutylammonium salt (tetrabutylammonium bromide (TBABr)) and fatty acids (malonic acid) to increase the sensitivity of OTC detection; the DES was prepared using a simple and green synthesis method. In this study, OTC was indirectly detected by decreasing the anodic peak current of F-AC in the presence of OTC. Modification of the SPE with F-AC combined with DES enhanced electrochemical sensitivity and selectivity for OTC detection. Various experimental parameters, including the modification of the electrode surfaces and the electrochemical behavior of OTC, were thoroughly investigated. Lastly, the proposed electrochemical sensor was successfully applied to determine OTC in shrimp pond samples.

2. MATERIALS AND METHODS

2.1. Chemicals and Reagents. All chemicals were of analytical grade. Oxytetracycline (OTC), tetracycline (TET), chlortetracycline (CTC), doxycycline (DOX), amoxicillin (AMOX), ciprofloxacin (CIP), and norfloxacin (NOR) were obtained from Sigma-Aldrich (Japan). *N,N*-dimethylformamide (DMF) was acquired from Sigma-Aldrich (Japan). Methanol was obtained from RCI Labscan (Thailand). Disodium hydrogen phosphate dihydrate and sodium dihydrogen phosphate dihydrate were obtained from QRëc (New Zealand). Potassium hexacyanoferrate(III) ($K_3Fe(CN)_6$) was obtained from Sigma-Aldrich (USA and Spain).

2.2. Apparatus. All electrochemical measurements were carried out using an electrochemical workstation (AutoLab, PGSTAT302N, Switzerland) containing 5 mL of the solution in a conventional three-electrode system at room temperature, using an SPE modified by fluorinated AC as the working electrode (F-AC/SPE), Ag/AgCl (3 mol L^{-1} NaCl) as the reference electrode (Hebei, China), and a platinum wire as the counter electrode (Hebei, China). The surface morphology and composition of the modified electrodes were examined using field-emission scanning electron microscopy (FESEM) and energy-dispersive X-ray spectroscopy (EDS) (Helios NanoLab G3 CX, FEI, USA). X-ray photoelectron spectroscopy (XPS; AXIS Ultra DLD, UK) was employed to analyze the elemental compositions of F and AC.

2.3. Fabrication of the Modified Electrodes. AC from waste coffee grounds was synthesized according to a previous study[18] and used as a precursor to synthesize F-AC. F-AC was carried out in accordance with a previous study[42] by mixing 1 mg of AC, 50 mL of ammonium hydroxide, and 200 mL of distilled water under vigorous stirring for 30 min at room temperature. Hydrofluoric acid (5 mL) was added to the solution, which was then stirred for 24 h at room temperature and filtered to separate the AC. The filtered AC was washed thrice with distilled water until a neutral solution (pH 7.0) was obtained. The prepared sample was dried for 24 h at 80 °C to obtain the final F-AC powder. F-AC (3 mg) was dissolved in DMF (1 mL) and sonicated for 30 min to obtain a homogenous suspension. The F-AC suspension (5 μL) was dropped onto the SPE surface, which was dried at room temperature to obtain F-AC/SPE. Before each measurement, a potential ranging from −1.0 to +1.0 V with a scan rate of 100
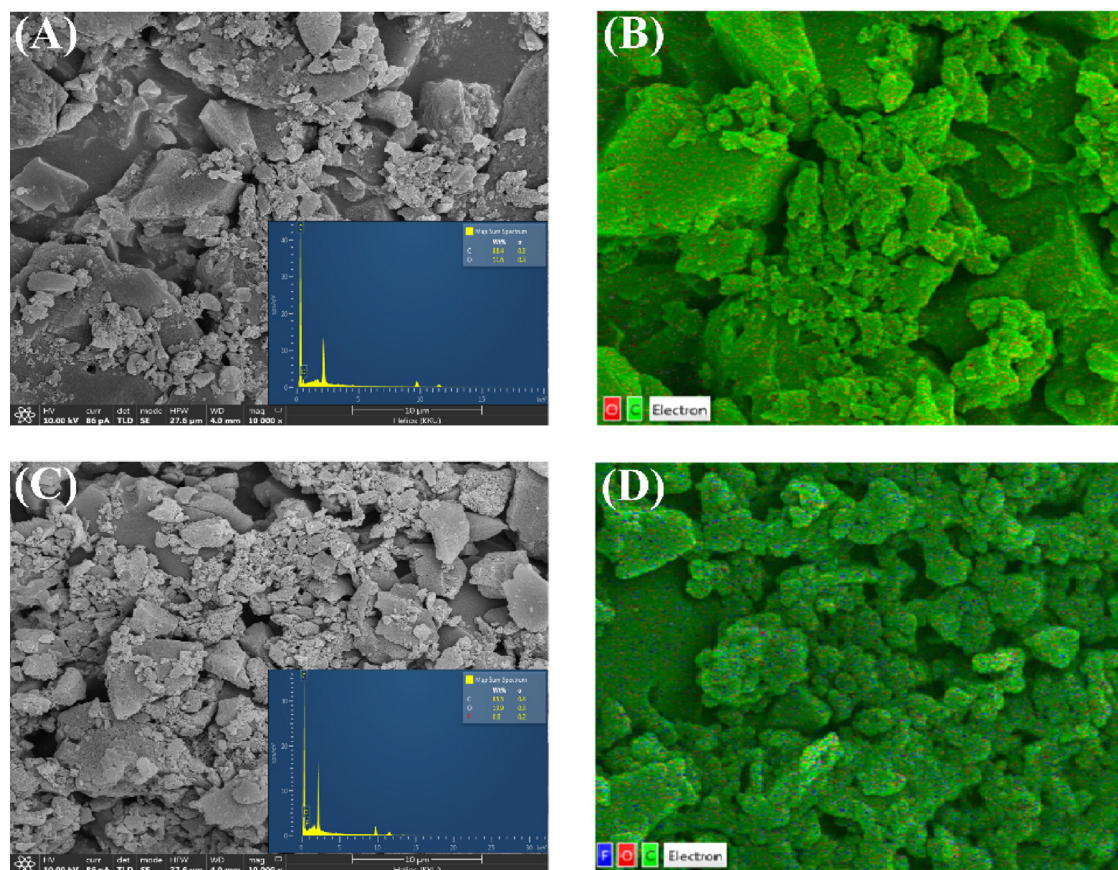
Figure 1. (A) FESEM image of AC (inset; EDS spectrum of AC), (B) EDS mapping of AC, (C) FESEM image of F-AC (inset; EDS spectrum of F-AC), and (D) EDS mapping of F-AC.

mV s^{-1} was applied to the modified electrode in a phosphate buffer (pH 7.0) and repeated for 20 cycles to clean the electrode surface. The phosphate buffer solutions were prepared in a pH range of 5.0−10.5 by mixing solutions of 0.1 mol L^{-1} NaH$_2$PO$_4$·2H$_2$O and 0.1 mol L^{-1} Na$_2$HPO$_4$·2H$_2$O. The pH of the acidic solution was adjusted by adding 0.1 mol L^{-1} H$_3$PO$_4$, while the addition of 0.1 mol L^{-1} NaOH was used to adjust the pH of the basic solution. All phosphate buffer solutions were stored at room temperature until the time of use in the electrochemical analysis.

DESs based on tetrabutylammonium bromide (TBABr) were studied with various fatty acids, including malonic acid (MA), tartaric acid (TA), oxalic acid (OA), phenylbutyric acid (PheBA), heptanoic acid (HepA), octanoic acid (OctA), and nanoic acid (NanoA). The DESs were prepared by mixing TBABr, fatty acids, and water in a molar ratio of 1:2:2, following which the mixture was heated at 80−90 °C in an oil bath under magnetic stirring (200 rpm) until homogeneity was obtained.[36] The prepared DESs were stored at room temperature until use.

2.4. Sample Preparation. Shrimp pond samples (WS−1−4) and shrimp samples (SH−1−4) were collected from a local market in Khon Kaen, Thailand. The shrimp pond samples were filtered through a 0.45 μm membrane before analysis. Meanwhile, shrimp samples were mixed until a homogeneous texture was obtained, accurately weighed (1.0000 g), and then placed in a 15 mL centrifuge tube to which McIlvain buffer (10 mL, pH 4.0) was added to extract the analyte. The samples were mixed by vortexing for 30 s and then centrifuged at 5000 rpm for 20 min. The resulting supernatant was filtered through

a 0.45 μm membrane before analysis using the proposed electrochemical sensor.

The McIlvain buffer solution (pH 4.0) was prepared by dissolving 7.5 g of disodium hydrogen phosphate dehydrate, 6.5 g of citric acid monohydrate, and 1.86 g of EDTA in water and diluting to 500 mL. The stock buffer solution was adjusted to pH 4.0 using 1 mol L^{-1} HCl.[6]

2.5. Electrochemical Analysis of Oxytetracycline. A 5 mL standard OTC or sample solution in phosphate buffer (pH 9.5) was detected by differential pulse voltammetry (DPV). The prepared DES (75 μL) was then added to each solution and stirred at 650 rpm for 20 s prior to electrochemical analysis using DES-F-AC/GCE. DPV measurements were performed from −1.0 to +0.6 V, and all experiments were performed in triplicate.

3. RESULTS AND DISCUSSION

3.1. Characterization of the Modified Electrode. The surface morphology and composition of AC/SPE and F-AC/SPE were characterized using SEM and EDS. Figure 1A shows the surface morphology of AC, which exhibits irregular shapes.[43] F-AC exhibits a surface morphology similar to that of AC and has a smooth surface, as shown in Figure 1C.[44,45] Moreover, EDS of the synthesized AC (inset; Figure 1A,B) displayed a composition of approximately 88% carbon atoms and 12% oxygen atoms, while that of F-AC/SPE displayed 49.5% carbon atoms, 41.6% oxygen atoms, and 0.6% fluorine atoms (inset; Figure 1C,D). Therefore, the successful fabrication of the proposed electrode was confirmed.
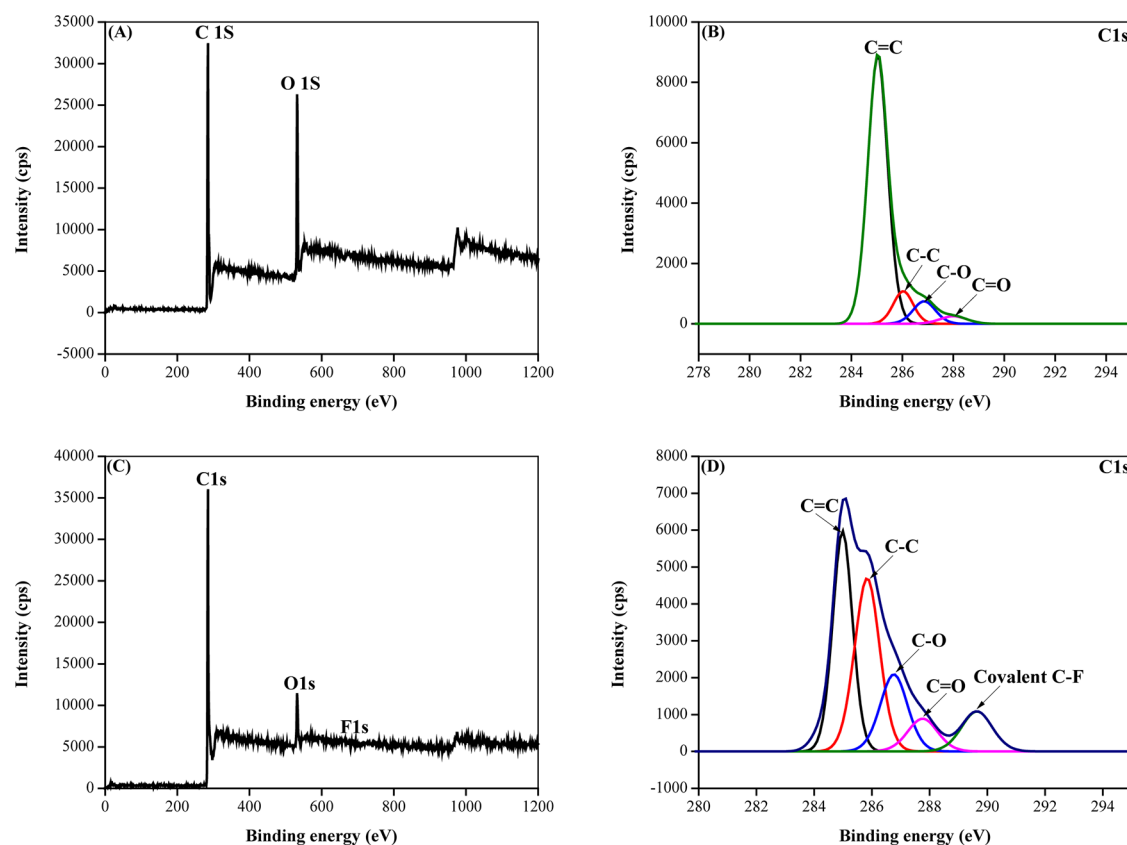
Figure 2. (A) XPS survey spectra of AC, (B) high-resolution C 1s spectra of AC, (C) XPS survey spectra of F-AC and (D) high-resolution C 1s spectra of F-AC.
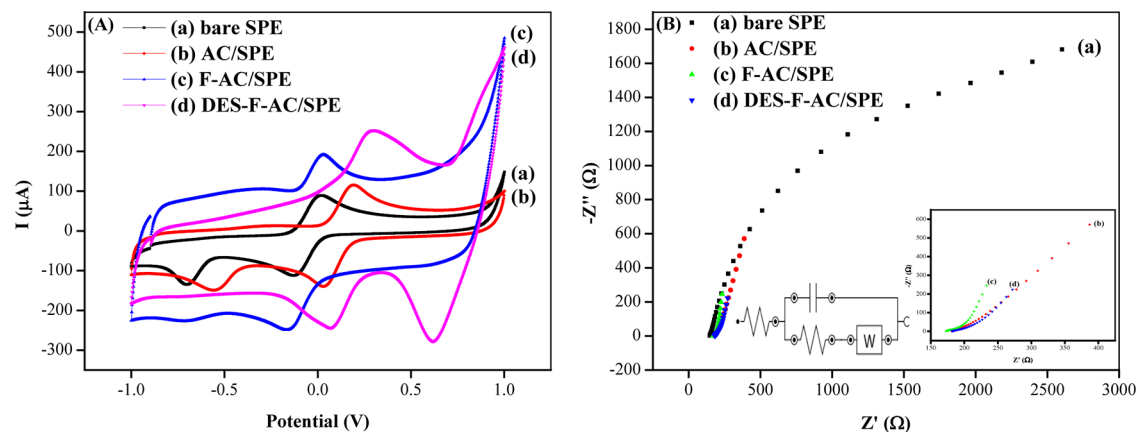

Figure 3. (A) Cyclic voltammograms of 5 mmol L^{-1} [Fe(CN)$_6$]$^{3-/4-}$ in 0.1 mol L^{-1} KCl at (a) bare GCE, (b) AC/SPE, (c) F-AC/SPE, and (d) DES-F-AC/SPE at a scan rate of 100 mV s^{-1}. (B) Nyquist plots of (a) bare SPE, (b) AC/SPE, (c) F-AC/SPE, and (d) DES-F-AC/SPE. Inset: Nyquist plots at (b) AC/SPE, (c) F-AC/SPE, and (d) DES-F-AC/SPE with the frequency ranging from 0.001 to 100 kHz and the Randles circuit model.

The synthesized AC and F-AC were characterized using XPS to study the chemical composition (Figure 2). The XPS spectrum of the synthesized AC (Figure 2A) displayed peaks at 285.0 and 532.0 eV, which indicated the presence of carbon and oxygen atoms, respectively. The high-resolution C 1s spectra of AC (Figure 2B) revealed C 1s peaks at the binding energies 285.0, 286.0, 287.0, and 288.0 eV, which correspond to C=C (sp^2 carbon), C−C, C−O, and C=O, respectively. The XPS spectrum of F-AC (Figure 2C), displayed peaks at binding energies of 285.0, 532.0, and 686.0 eV, which indicated the presence of carbon, oxygen, and fluorine atoms,

respectively. Figure 2D illustrates the high-resolution C 1s spectra of F-AC, wherein an additional peak corresponding to the C−F bond (289.8 eV) was observed, which was not detected for AC.[46] The relatively high C−F binding energy was due to the large electronegativity difference between the components; the electronegativity difference enhanced the conductivity of the activated carbon by facilitating charge transfer between fluorine and carbon.[47,48] Thus, the XPS results revealed that the doping of fluorine atoms on AC was successful in fabricating F-AC.

3.2. Electrochemical Behavior of Modified Electrodes.

The electrochemical efficiencies of the modified electrodes were characterized by cyclic voltammetry (CV) and electrochemical impedance spectroscopy (EIS) in 5 mmol L^{-1} $[Fe(CN)_6]^{3-/4-}$ containing 0.1 mol L^{-1} KCl. As shown in Figure 3A, the response of $[Fe(CN)_6]^{3-/4-}$ at bare SPE was the lowest value including the peak separation (ΔE) of 0.20 V at bare SPE obtained from the anodic peak at 0.00 V and the cathodic peak at −0.20 V and current of $[Fe(CN)_6]^{3-/4-}$ due to a small surface area (0.069 cm^2) and weak conductivity. After the modification with either AC or F-AC (AC/SPE and F-AC/SPE), the peak currents were clearly increased and the peak potentials were shifted to a negative value providing ΔE of 0.18 and 0.15 V for AC/SPE and F-AC/SPE, respectively. Furthermore, when F-AC combined with DESs (DES-F-AC/SPE), the response of $[Fe(CN)_6]^{3-/4-}$ showed the highest peak current resulting from the synergistic effect of F-AC and DES. The ΔE of 0.15 V was obtained from DES-F-AC/SPE and another one peak at 0.65 V (cathodic peak) was the peak potential of the DES, indicating that electron transfer was facilitated.

According to the Randles−Sevcik equation,[49] the electroactive surface area can also be calculated as

$$I_p = 2.69 \times 10^5 n^{3/2} A D^{1/2} \nu^{1/2} C_p \tag{1}$$

where I_p is the peak current (A), n is the number of electrons transferred in the reaction, A is the active surface area (cm^2), D is the diffusion coefficient (7.6×10^{-6} cm^2 s^{-1}), ν is the scan rate (V s^{-1}), and C_p is the concentration of the redox species $[Fe(CN)_6]^{3-/4-}$ (5.0 mmol L^{-1}). The effective surface areas of bare SPE, AC/SPE, F-AC/SPE, and DES-F-AC/SPE were estimated to be 0.069, 0.074, 0.078, and 0.110 cm^2, respectively. The DES-F-AC/SPE showed the highest electrochemical response because (i) F-AC has a high surface area and sp^2 hybridized carbon atoms constitute the main structure, leading to a much lower electron transfer resistance and high conductivity, and (ii) the presence of DES induced more porosity in F-AC, thus increasing the surface area for target analyte adsorption. Furthermore, the high conductivity of the DES accelerated the electron transfer between the analyte and electrode surface.[50]

EIS was used to study the interfacial properties of the surface-modified electrodes. A modified Randles circuit was chosen to fit the impedance data. The circuit parameters corresponding to the electron transfer resistance (R_{ct}) and Warburg impedance are both parallel to the double-layer capacitance. Figure 3B shows the impedance spectra of (a) bare SPE, (b) AC/SPE, (c) F-AC/SPE, and (d) DES-F-AC/SPE. The R_{ct} at the SPE was evaluated to be 54.6 Ω, which dropped to 7.97 Ω at the AC/SPE and 4.94 Ω at the F-AC/SPE. DES-F-AC/SPE exhibited the lowest R_{ct} of 3.14 Ω. Therefore, the decrease in R_{ct} proves the significant acceleration of electron transfer by DESs and F-AC. The impedance results confirmed the successful fabrication of DES-F-AC on the bare SPE surface.

The electrochemical properties of OTC on F-AC/SPE and DES-F-AC/SPE were studied by CV. A comparison of the electrochemical behavior of OTC on F-AC/SPE and DES-F-AC/SPE is shown in Figure 4. The F-AC/SPE (inset A) and DES-F-AC/SPE (inset B) cyclic voltammograms demonstrated the oxidation reaction of F-AC at an anodic peak potential (E_{pa}) of ~0.30 V.[51] The decrease in the current (ΔI) of AC in
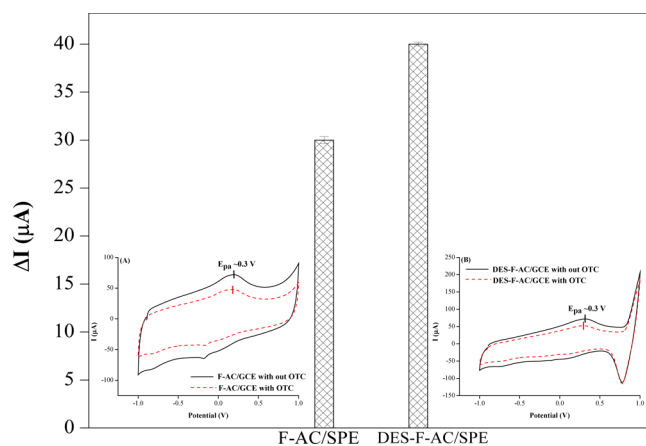

Figure 4. Comparison of OTC electrochemical behavior on F-AC/SPE (inset A; cyclic voltammograms of F-AC/SPE with and without 200 μg L^{-1} OTC) and DES-F-AC/SPE (inset B; cyclic voltammograms of DES-F-AC/SPE with and without 200 μg L^{-1} OTC) at E_{pa} of 0.3 V in 0.1 mol L^{-1} phosphate buffer (pH 7.0) at a scan rate of 100 mV s^{-1}.

the presence of OTC was compared to that without OTC. The ΔI of AC on DES-F-AC/SPE was higher than that on F-AC/SPE owing to the adsorption of OTC on the surface of F-AC through electrostatic interactions, hydrogen bonding, and π−π interactions, as shown in Figure 5.[52]

The adsorption mechanism of OTC on the electrode surface was investigated based on the effect of the scan rate (ν) on the peak current and potential at the F-AC/SPE. The CV curves of F-AC/SPE were obtained at different scan rates over the range 10−100 mV s^{-1} in the presence of 200 μg L^{-1} OTC (Figure S1A). The peak current of the AC increased, and the potential shifted with increasing scan rate, confirming the irreversibility of the electrode process.[53] The relationship between the change in current (ΔI) and the scan rate (ν) was linear, with a regression equation of $\Delta I = 0.0041\nu + 0.0518$ ($R^2 = 0.9973$), as shown in Figure S1B. The relationship between the peak potential and scan rate is based on the Laviron equation:[54]

$$E_p = E^0 + (RT/\alpha nF) \ln(RTk^0/\alpha nF) + (RT/\alpha nF) \ln\nu \tag{2}$$

where E_p is the peak potential, E^0 is the formal potential (V), T is the temperature (298.15 K), α is the electron transfer coefficient, n is the electron transfer number, k^0 is the rate constant, F is the Faraday constant ($F = 96,485$ C mol^{-1}, $R = 8.314$ J K^{-1} mol^{-1}), and ν is the scan rate (V s^{-1}). The relationship between the oxidation peak potential (E_{pa}) and the natural logarithm of the scan rate ($\ln\nu$) is shown in Figure S1C. The oxidation peaks moved directly toward a positive potential for various scanning rates. E_{pa} was linearly proportional to $\ln \nu$ and could be described by the linear equation $E_p = 0.085 \ln\nu + 0.0514$ ($R^2 = 0.9902$). The slope of E_p against $\ln\nu$ was calculated according to eq 2; a calculated value of 0.30 was achieved for αn, with α being assumed as 0.5 for the irreversible progress.[55] Therefore, the number of electrons in the OTC oxidation reaction was evaluated to be 1, which is consistent with previous reports.[56] The reaction between OTC and F-AC/SPE is shown in Figure 5.

3.3. Optimization of Experimental Parameters.

3.3.1. Effect of Concentration and Volume of F-AC.

In this study, the electrochemical behavior of OTC adsorbed on modified electrodes was studied using CV and DPV. The peak
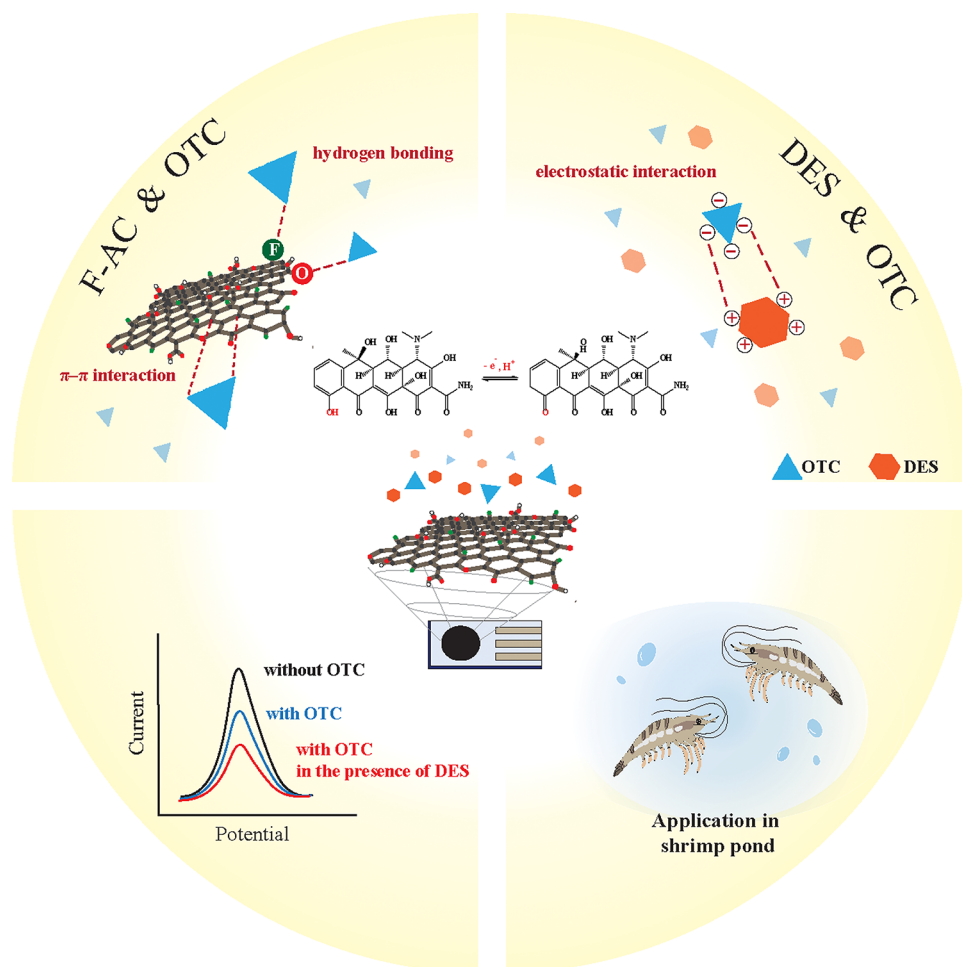
Figure 5. Schematic diagram of the F-AC/SPE and DES-F-AC/SPE sensors for the detection of OTC.

current of F-AC decreased significantly owing to the adsorption of OTC on the surface of the electrode through electrostatic interactions, hydrogen bonding, and π–π electron donor–acceptor interactions.[52] Therefore, the results were investigated based on the change in the current (ΔI) of F-AC with and without OTC. Although OTC affected the oxidation peaks of F-AC, only the oxidation peak (anodic current) of F-AC was considered.

The effect of the concentration and volume of the F-AC suspension on the modified electrode (F-AC/SPE) was studied over the ranges 1−10 mg/mL and 2−10 μL, respectively; the effect of F-AC concentration is presented in Figure S2A and the effect of the F-AC volume in Figure S2B. It was found that the ΔI of F-AC/SPE increased slightly with an increase in the concentration of the F-AC suspension from 1 to 3 mg mL^{-1}; above this concentration (>3 mg mL^{-1}), the ΔI of F-AC decreased slightly. Meanwhile, the ΔI of F-AC increased as the volume of the F-AC suspension increased from 2 to 5 μL; further increase in the volume (>5 μL) caused a decrease in the ΔI. The ΔI of F-AC decreased when the concentration and volume of F-AC increased beyond 3 mg mL^{-1} and 5 μL, respectively, because the thick layer of F-AC blocked the electron transfer from the F-AC to the electrode surface. Therefore, the optimum concentration and amount of F-AC were selected as 3 mg mL^{-1} and 5 μL, respectively.

3.3.2. Effect of DESs. The effects of DESs including type, mole ratio, and volume of DESs were also investigated by DPV. The effect of various type of DES-based TBABr (hydrogen bond acceptor) with different fatty acids (hydrogen bond donor) including MA, TA, OA, PheBA, HepA, OctA, or NanoA is shown in Figure S3A, TBABr:MA gave the highest ΔI of F-AC in the presence of 200 μg L^{-1} OTC in 0.1 mol L^{-1} phosphate buffer (pH 9.5), whereas the results of TBABr:TA and TBABr:OA were not shown because they were not be synthesized. Thus, TBABr:MA was chosen for further experiment. The TBABr:MA mole ratio was also studied, and the result is shown in Figure S3B. For TBABr:MA, 2:1 is the optimum ratio to form DESs, which gave highest ΔI of F-AC. It is because the high ratio of TBABr causes a high positive charge to interact with anionic charge of OTC. The DES volume was studied in range of 50−125 μL, as shown in Figure S3C. The ΔI increased until the DES volume up to 75 μL. After this, the ΔI was decreased because DES covered the F-AC surface. The DES hindered the electrochemical behavior between OTC and the surface of electrodes. Therefore, the optimum DES volume is 75 μL.

3.3.3. Effect of pH. The influence of pH on the DES system was studied over a pH range of 8.5−10.5 at DES-F-AC/SPE using 0.1 mol L^{-1} phosphate buffer. The results (Figure S4A) showed that ΔI increased until pH 9.5 and then sharply decreased. DES is of the ionic hydrophobic type that acts as a highly efficient extractant for a wide range of compounds.[57] At pH < pK_{a3}, OTC has one positive charge, one zwitterion, and one negative charge, which interact poorly with the cationic
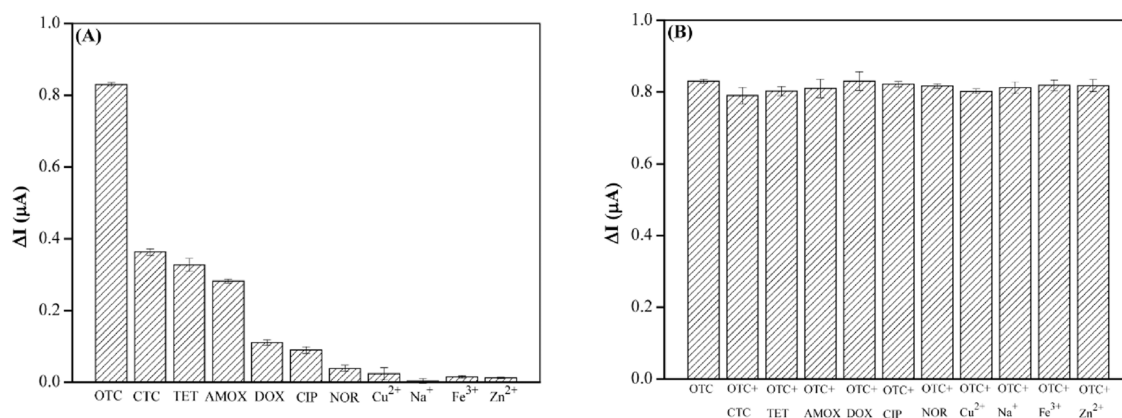
Figure 6. Selectivity of the DES-F-AC/SPE (A) with various antibiotics and metal ions (200 μg L^{-1} of each) and (B) containing 200 μg L^{-1} OTC and in individual addition of 200 μg L^{-1} another antibiotic and metal ions. All experiments were carried out in 0.1 mol L^{-1} phosphate buffer (pH 9.5).

DES. However, at pH > pK_{a3}, OTC produced two negative charges and was fully deprotonated; thus, the sensitivity of OTC increased owing to the electrostatic interactions between the anionic OTC and the cationic DES. Hence, a phosphate buffer with a pH of 9.5 was chosen for the DES-F-AC/SPE system.

Moreover, the number of protons and electrons transferred in the reaction of OTC were investigated using F-AC/SPE in the pH range of 5.0−7.5. At low pH values, OTC was positively charged (pH < pK_{a1} (3.6)). One negative charge was obtained for OTC at pH values higher than that of pK_{a2} (>7.3). At high pH values, OTC had two negative charges (pH > pK_{a3} (8.9)). At pH values ranging between pK_{a1} and pK_{a2}, OTC molecules existed in neutral or zwitterionic forms.[55] Fig-Figure S4B,C shows the influence of pH on the peak current and ΔI of F-AC, respectively, in the presence of OTC. It was found that the peak intensity and ΔI increased with increasing pH until pH 6.0, and thereafter significantly decreased. Moreover, the voltammograms showed that when the pH decreased, the anodic and cathodic peak potentials of F-AC were more positive, suggesting the involvement of protons in the oxidation of OTC. At pH 6.0, the zwitterion OTC was easily oxidized, and the maximum peak current of AC was achieved. According to the Nernst equation,[49] the relationship between E_p and pH is described as:

$$E_p = \frac{0.0592m}{n} \text{pH} + b \tag{3}$$

where E_p is the peak potential (V), m and n are the numbers of protons and electrons in the electrochemical reaction, respectively, and b is the intercept of the equation. Plots of the peak potential (E_p) and pH (Figure S4D) revealed that the linear relationship can be expressed as follows: E_p = −0.0690pH + 0.9099 (R^2 = 0.9988). It is clearly seen that the linear slope, 69.0 mV pH^{-1}, is close to the theoretical value, 59.2 mV pH^{-1},[58] implying that the numbers of protons and electrons transferred in the reaction of OTC were equal.

3.3.4. Selectivity of OTC Detection. To evaluate the selectivity of the fabricated sensor, the effect of potential interference from species such as antibiotics (amoxicillin, tetracycline, doxycycline, chlortetracycline, ciprofloxacin, and norfloxacin) and cations (Cu^{2+}, Fe^{3+}, Na$^+$, and Zn^{2+}) were studied by DPV using the DES-F-AC/SPE containing 200 μg L^{-1} of OTC and 200 μg L^{-1} of antibiotics and cations. The

results clearly showed that all studied substances did not significantly interfered MP detection (Figure 6A), while CTC, DOX, and TET had an effect on the DPV signal, which may be because these compounds are in the same chemical group as OTC. The selectivity of the modified electrodes for OTC detection using another antibiotic and metal ions containing OTC at the same concentration is shown in Figure 6B. The results showed that the change in the F-AC signal was still ≥95%. Thus, OTC exhibited the highest sensitivity under the studied conditions for the fabricated electrochemical sensor.

3.4. Quantitative Analysis and Method Validation. The analytical performance of the fabricated sensor, DES-F-AC/SPE, was evaluated using DPV under optimal conditions. The analytical features studied were the linearity, detection limit (LOD), and quantification limit (LOQ). Figure 7 displays the voltammograms of F-AC recorded in a potential range of −1.0 to +1.0 V in different OTC concentrations using the proposed electrochemical sensors. The current corresponding to F-AC decreased with increasing OTC concentration from 0 to 1500 μg L^{-1}. The results obtained from the DES-F-AC/SPE ranged from 5 to 1500 μg L^{-1} and displayed linearity, with a
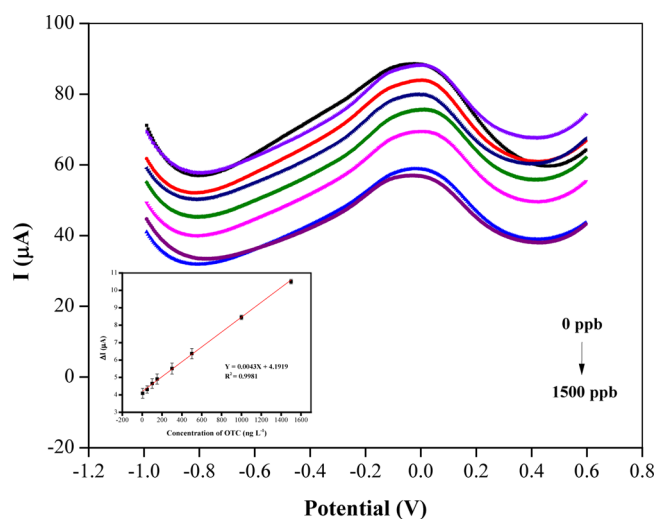

Figure 7. Differential pulse voltammograms of F-AC in the presence of different concentrations of OTC in 0.1 mol L^{-1} phosphate buffer pH 6.0 at the DES-F-AC/SPE. Inset: calibration plot of DES-F-AC/SPE sensors obtained from DPV measurement.

Table 1. Comparison of the Proposed Sensor (DES-F-AC/SPE) with Other Sensors for OTC Detection

modified electrode	sample	linear range ($\mu g\ L^{-1}$)	LOD ($\mu g\ L^{-1}$)	%recovery	analytical method	reference
PoAP/MWCNTs/Pt[a]	pharmaceutical formulations	90−1500	46.00	96.9−103.5%	CV	59
Zn-Mt/GCE[b]	chicken feed, chicken, fish, and shrimp	370−18,000	55.25	95.8−104.0%	DPV	60
Cu$_2$O microsphere/GCE[c]	animal-derived food	230−9700	69.00	97.4−107.0%	SWV	61
Ta$_2$O$_5$-ErGO/GCE[d]	milk	90−4600	43.74	100.1−120.9%	CV	57
DES-F-AC/SPE	shrimp pond and shrimp samples	5−1500	1.74	83.8−105.0%	DPV	this work

Table 2. Recovery Studies of Spiked OTC in Shrimp Pond Samples (n = 3)

	WS-1			WS-2			WS-3			WS-4		
spiked ($\mu g\ L^{-1}$)	found ($\mu g\ L^{-1}$)	% recovery	% RSD	found ($\mu g\ L^{-1}$)	% recovery	% RSD	found ($\mu g\ L^{-1}$)	% recovery	% RSD	found ($\mu g\ L^{-1}$)	% recovery	% RSD
6.00	5.61	93.5	1.14	5.25	87.5	9.57	5.71	95.2	4.19	5.77	96.2	1.82
500	453	90.7	0.32	419	83.8	2.56	486	97.1	0.30	494	98.8	5.23
1000	983	98.3	1.75	1005	100.5	0.76	952	95.2	0.28	986	98.6	4.48
HPLC analysis at 500 $\mu g\ L^{-1}$	529	105.9	8.04	496	99.2	3.65	481	96.2	0.39	433	86.5	6.09
HPLC analysis at 1000 $\mu g\ L^{-1}$	1027	102.7	2.36	954	95.4	0.44	992	99.2	2.36	969	96.9	1.32

Table 3. Recovery Studies of Spiked OTC in Shrimp Samples (n = 3)

	SH-1			SH-2			SH-3			SH-4		
spiked ($\mu g\ L^{-1}$)	found ($\mu g\ L^{-1}$)	% recovery	% RSD	found ($\mu g\ L^{-1}$)	% recovery	% RSD	found ($\mu g\ L^{-1}$)	% recovery	% RSD	found ($\mu g\ L^{-1}$)	% recovery	% RSD
6.00	7.53	94.1	4.00	8.20	101.4	6.67	7.20	93.3	2.11	7.25	101.1	2.38
500	518	103.1	1.08	502	99.9	0.58	509	101.4	0.40	513	102.5	1.73
1000	1047	104.5	1.05	1028	102.6	1.60	1032	103.4	0.65	1039	103.7	1.27
HPLC analysis at 500 $\mu g\ L^{-1}$	530	106.0	6.59	515	103.0	6.32	509	101.9	4.56	504	100.8	0.93
HPLC analysis at 1000 $\mu g\ L^{-1}$	1011	101.1	1.30	1014	101.4	1.48	958	95.8	6.47	934	93.4	0.83

determination coefficient (R^2) of 0.9981 (inset; Figure 7). The LOD and LOQ were calculated according to the following equations: LOD = $3\sigma/S$ and LOQ = $10\sigma/S$, where σ is the standard deviation of the blank (n = 7) and S is the slope of the calibration plot. The LOD and LOQ obtained from the DES-F-AC/SPE were 1.74 and 5.80 $\mu g\ L^{-1}$, respectively. The results indicated that the DES-F-AC/SPE exhibited a high sensitivity for OTC detection. In addition, the performance of the DES-F-AC/SPE sensor was compared with that of previously reported sensors, as summarized in Table 1. While the linear range of the fabricated sensor was comparable to that of other sensors, this sensor was more sensitive than most reported sensors, which provided a low LOD. In addition, the proposed sensor DES-F-AC/SPE is simple to fabricate and cost-effective.

[a]PoAP/MWCNTs/Pt: Poly-ortho-aminophenol and multi-walled carbon nanotubes deposited on the platinum electrode.

[b]Zn-Mt/GCE: Zinc cation-exchanged montmorillonite-modified glassy carbon electrode.

[c]Cu$_2$O microsphere/GCE: copper(I) oxide microsphere-modified glassy carbon electrode.

[d]Ta$_2$O$_5$-ErGO/GCE: Tantalum pentoxide nanoparticle-electrochemically reduced graphene oxide nanocomposite-modified glassy carbon electrode.

3.5. Detection of OTC in Real Samples. The performance of the DES-F-AC/SPE sensor in detecting OTC in shrimp pond and shrimp samples was tested. In this work, to ensure that the sensor exhibited a high performance for the detection of OTC, AC was modified by doping with fluorine atoms and the electrical conductivity was increased using DESs. The detection of OTC occurred through the electrostatic interactions between DES and OTC under alkaline conditions and the adsorption of OTC on the F-AC surface through H-bonding and $\pi-\pi$ interactions. The OTC in shrimp samples was extracted by adding the McIlvaine buffer (pH 4.0). Shrimp pond and shrimp samples were spiked with OTC at three concentration levels (6, 500, and 1000 $\mu g\ L^{-1}$), and the detection was performed in triplicate. The recoveries of OTC were achieved in the range of 83.8−100.5% and 93.3−104.5% for the water samples from the shrimp pond and shrimp samples, respectively. The RSDs of OTC detection in all samples was less than 6.70%, as shown in Tables 2 and 3. The results from the fabricated sensor at 500 and 1000 ng L^{-1} OTC were compared with those from HPLC and were in good agreement. Thus, the fabricated sensor (DES-F-AC/SPE) effectively and accurately detected OTC.

4. CONCLUSIONS

A novel and sensitive electrochemical sensor using the SPE modified with F-AC in the presence of DES (DES-F-AC/SPE) was fabricated to detect OTC. The facile doping of AC with fluorine increased its surface area and conductivity. Moreover, the novel DES made from TBABr and malic acid increased the sensitivity of F-AC for the detection of OTC, while also inducing preconcentration of OTC to increase its detectability. OTC determination was achieved through electrostatic interactions between DES and OTC, which facilitated adsorption of OTC on the F-AC surface through H-bonding and $\pi-\pi$ interactions. The electrochemical sensor exhibited an

excellent response toward OTC, with an LOD of 1.74 μg L^{-1}. In addition to its ease and low-cost fabrication, this proposed innovative sensor can be considered to be eco-friendly owing to the use of a green solvent (DES). Lastly, the DES-F-AC/SPE was successfully applied for the detection of OTC in water samples from shrimp pond and shrimp samples, with satisfactory recoveries of 83.8−100.5% and 93.3−104.5%, respectively.

ASSOCIATED CONTENT

Supporting Information

The Supporting Information is available free of charge at https://pubs.acs.org/doi/10.1021/acsomega.2c06462.

Effect of scan rates, effect of concentration and volume of F-AC, effect of DES, and effect of pH (PDF)

AUTHOR INFORMATION

Corresponding Author

Siriboon Mukdasai − Materials Chemistry Research Center, Department of Chemistry and Center of Excellence for Innovation in Chemistry, Faculty of Science, Khon Kaen University, Khon Kaen 40002, Thailand; orcid.org/0000-0002-4587-4372; Email: sirimuk@kku.ac.th

Authors

Narumon Wannasri − Materials Chemistry Research Center, Department of Chemistry and Center of Excellence for Innovation in Chemistry, Faculty of Science, Khon Kaen University, Khon Kaen 40002, Thailand

Pikaned Uppachai − Department of Applied Physics, Faculty of Engineering, Rajamangala University of Technology Isan, Khon Kaen 40000, Thailand

Kompichit Seehamart − Department of Applied Physics, Faculty of Engineering, Rajamangala University of Technology Isan, Khon Kaen 40000, Thailand

Sakwiboon Jantrasee − Department of Applied Physics, Faculty of Engineering, Rajamangala University of Technology Isan, Khon Kaen 40000, Thailand

Nuttaya Butwong − Applied Chemistry Department, Faculty of Sciences and Liberal Arts, Rajamangala University of Technology Isan, Nakhon Ratchasima 30000, Thailand

Kanit Mukdasai − Department of Mathematics, Faculty of Science, Khon Kaen University, Khon Kaen 40002, Thailand

Illyas Md Isa − Department of Chemistry, Faculty of Science and Mathematics, Universiti Pendidikan Sultan Idris, Tanjong Malim, Perak 35900, Malaysia

Complete contact information is available at:
https://pubs.acs.org/10.1021/acsomega.2c06462

Author Contributions

N.W. contributed to the conceptualization, methodology, investigation, and writing of the original draft. P.U. contributed in methodology, validation, and visualization. K.S., S.J., K.M., and I.M.I. carried out the visualization. N.B. did the validation and visualization. S.M. contributed to the conceptualization, supervision, and writing—review and editing.

Notes

The authors declare no competing financial interest.

ACKNOWLEDGMENTS

REFERENCES

(1) Muriuki, F. K.; Ogara, W. O.; Njeruh, F. M.; Mitema, E. S. Tetracycline residue levels in cattle meat from Nairobi salughter house in Kenya. J. Vet. Sci. 2001, 2, 97−101.

(2) Hou, H.; Bai, X.; Xing, C.; Gu, N.; Zhang, B.; Tang, J. Aptamer-based cantilever array sensors for oxytetracycline detection. Anal. Chem. 2013, 85, 2010−2014.

(3) Halling-Sørensen, B.; Sengeløv, G.; Tjørnelund, J. Toxicity of tetracyclines and tetracycline degradation products to environmentally relevant bacteria, including selected tetracycline-resistant bacteria. Arch. Environ. Contam. Toxicol. 2002, 42, 263−271.

(4) Rafati, L.; Ehrampoush, M. H.; Mokhtari, M.; Sohrabi, A.; Shirazi, S.; Mahvi, A. H.; Momtaz, S. M. The analysis of oxytetracycline residue in tissues of cultured rainbow trout (Oncorhynchus Mykiss). Health Scope 2017, 7, No. e57495.

(5) Smyrniotakis, C. G.; Archontaki, H. A. C18 columns for the simultaneous determination of oxytetracycline and its related substances by reversed-phase high performance liquid chromatography and UV detection. J. Pharm. Biomed. Anal. 2007, 43, 506−514.

(6) Alanazi, F.; Almugbel, R.; Maher, H. M.; Alodaib, F. M.; Alzoman, N. Z. Determination of tetracycline, oxytetracycline and chlortetracycline residues in seafood products of Saudi Arabia using high performance liquid chromatography-Photo diode array detection. Saudi Pharm. J. 2021, 29, 566−575.

(7) Lin, Y. H.; Lu, F.; Wang, J. Disposable carbon nanotube modified screen-printed biosensor for amperometric detection of organophosphorus pesticides and nerve agents. Electroanalysis 2004, 16, 145−149.

(8) Oliveira, G. G.; Janegitz, B. C.; Zucolotto, V.; Fatibello, O. Differential pulse adsorptive stripping voltammetric determination of methotrexate using a functionalized carbon nanotubes-modified glassy carbon electrode. Cent. Eur. J. Chem. 2013, 11, 1837−1843.

(9) Ardila, J. A.; Oliveira, G. G.; Medeiros, R. A.; Fatibello, O. Square-wave adsorptive stripping voltammetric determination of nanomolar levels of bezafibrate using a glassy carbon electrode modified with multi-walled carbon nanotubes within a dihexadecyl hydrogen phosphate film. Analyst 2014, 139, 1762−1768.

(10) Li, G.; Xia, Y.; Tian, Y.; Wu, Y.; Liu, J.; He, Q.; Chen, D. Recent developments on graphene-based electrochemical sensors toward nitrite. J. Electrochem. Soc. 2019, 166, 881−895.

(11) Huang, H.; Chen, L.; Wang, S.; Kang, P.; Chen, X.; Guo, Z.; Huang, X.-J. Electrochemical monitoring of persistent toxic substances using metal oxide and its composite nanomaterials: design, preparation, and application. TrAC Trends Analyt. Chem. 2019, 119, No. 115636.

(12) Zhou, M.; Han, L.; He, H.; Deng, D.; Zhang, L.; Yan, X.; Wu, Z.; Zu, Y.; Luo, L. Sensitive and selective determination of Cu^{2+} using self-assembly of 4-mercaptobenzoic acid on gold nanoparticles. J. Anal. Test. 2019, 3, 306−312.

(13) Mazloum-Ardakani, M.; Alizadeh, Z.; Sabaghian, F.; Mirjalili, B.; Salehi, N. Novel Fe$_2$O$_3$@CeO$_2$ Coreshell-based electrochemical nanosensor for the voltammetric determination of norepinephrine. Electroanalysis 2020, 32, 455−461.

(14) Cai, Z.; Ye, Y.; Wan, X.; Liu, J.; Yang, S.; Xia, Y.; Li, G.; He, Q. Morphology dependent electrochemical sensing properties of iron oxide-graphene oxide nanohybrids for dopamine and uric acid. Nanomaterials 2019, 9, 835.

(15) Li, G.; Wu, J.; Jin, H.; Xia, Y.; Liu, J.; He, Q.; Chen, D. Titania/electro-reduced graphene oxide nanohybrid as an efficient electrochemical sensor for the determination of allura red. Nanomaterials 2020, 10, 307.

(16) Chen, S.; Yuan, R.; Chai, Y.; Hu, F. Electrochemical sensing of hydrogen peroxide using metal nanoparticles: a review. *Microchim. Acta* **2013**, *180*, 15−32.

(17) Zakaria, R.; Jamalluddin, N. A.; Bakar, M. Z. A. Effect of impregnation ratio and activation temperature on the yield and adsorption performance of mangrove based activated carbon for methylene blue removal. *Results Mater.* **2021**, *10*, No. 100183.

(18) Wannasri, N.; Uppachai, P.; Butwong, N.; Jantrasee, S.; Isa, I. M.; Loiha, S.; Srijaranai, S.; Mukdasai, S. A facile nonenzymatic electrochemical sensor based on copper oxide nanoparticles deposited on activated carbon for the highly sensitive detection of methyl parathion. *J. Appl. Electrochem.* **2022**, *52*, 595−606.

(19) Wang, Z.; Sun, G.; Routh, P.; Kim, D. H.; Huang, W.; Chen, P. Heteroatom-doped graphene materials: syntheses, properties and applications. *Chem. Soc. Rev.* **2014**, *43*, 7067−7098.

(20) Wang, D. W.; Su, D. Heterogeneous nanocarbon materials for oxygen reduction reaction. *Energy Environ. Sci.* **2014**, *7*, 576−591.

(21) Li, Y.; Wang, J.; Li, X.; Liu, J.; Geng, D.; Yang, J.; Li, R. Nitrogen-doped graphene nanosheets as cathode materials with excellent electrocatalytic activity for high capacity lithium-oxygen batteries. *Electrochem. Commun.* **2012**, *18*, 12−15.

(22) Choi, C. H.; Park, S. H.; Woo, S. I. Binary and ternary doping of nitrogen, boron, and phosphorus into carbon for enhancing electrochemical oxygen reduction activity. *ACS Nano* **2012**, *6*, 7084−7091.

(23) Sheng, Z. H.; Gao, H. L.; Bao, W. J.; Wang, F. B.; Xia, X. H. Synthesis of boron doped graphene for oxygen reduction reaction in fuel cells. *J. Mater. Chem.* **2012**, *22*, 390−395.

(24) Zhao, Y.; Yang, L.; Chen, S.; Wang, X.; Ma, Y.; Wu, Q.; Jiang, Y.; Qian, W.; Hu, Z. Can boron and nitrogen co-doping improve oxygen reduction reaction activity of carbon nanotubes? *J. Am. Chem. Soc.* **2013**, *135*, 1201−1204.

(25) Yang, D. S.; Bhattacharjya, D.; Inamdar, S.; Park, J.; Yu, J. S. Phosphorus-doped ordered mesoporous carbons with different lengths as efficient metal-free electrocatalysts for oxygen reduction reaction in alkaline media. *J. Am. Chem. Soc.* **2012**, *134*, 16127−16130.

(26) Yu, D.; Xue, Y.; Dai, L. Vertically aligned carbon nanotube arrays co-doped with phosphorus and nitrogen as efficient metal-free electrocatalysts for oxygen reduction. *J. Phys. Chem. Lett.* **2012**, *3*, 2863−2870.

(27) Nakajima, T.; Koh, M.; Gupta, V.; Zemva, B.; Lutar, K. Electrochemical behavior of graphite highly fluorinated by high oxidation state complex fluorides and elemental fluorine. *Electrochim. Acta* **2000**, *45*, 1655−1661.

(28) Li, B.; Zhou, L.; Wu, D.; Peng, H.; Yan, K.; Zhou, Y.; Liu, Z. Photochemical chlorination of graphene. *ACS Nano* **2011**, *5*, 5957−5961.

(29) Hasan, M.; Meiou, W.; Wang, L.; Yulian, S.; Ullah, H. Q.; Ta, L.; Zhao, R. G.; Mendes, Z. P.; Malik, R. M.; Amed, Z.; Liu, Z.; Rummeli, M. H. Direct chemical vapor deposition synthesis of large area single-layer brominated graphene. *RSC Adv.* **2019**, *9*, 13527−13532.

(30) Kalita, G.; Wakita, K.; Takahashi, M.; Umeno, M. Iodine doping in solid precursor-based CVD growth graphene film. *J. Mater. Chem.* **2011**, *21*, 15209−15213.

(31) Zhou, J.; Lian, J.; Hou, L.; Zhang, J.; Gou, H.; Xia, M.; Zhao, Y.; Strobel, T. A.; Tao, L.; Gao, F. Ultrahigh volumetric capacitance and cyclic stability of fluorine and nitrogen co-doped carbon microspheres. *Nat. Commun.* **2015**, *6*, 8503.

(32) Zhou, H.; Peng, Y.; Wu, H.; Sun, F.; Yu, H.; Liu, F.; Xu, Q.; Lu, Y. Fluorine-rich nanoporous carbon with enhanced surface affinity in organic electrolyte for high performance supercapacitors. *Nano Energy* **2016**, *21*, 80−89.

(33) Wang, T.; Zang, X.; Wang, X.; Gu, X.; Shao, Q.; Cao, N. Recent advances in fluorine doped/fluorinated carbon-based materials for supercapacitors. *Energy Storage Mater.* **2020**, *30*, 367−384.

(34) Smith, E. L.; Abbott, A. P.; Ryder, K. Deep eutectic solvents (DESs) and their applications. *Chem. Rev.* **2014**, *114*, 11060−11082.

(35) Hayyan, M.; Hashim, M. A.; Hayyan, A.; Al-Saadi, M. A.; AlNashef, I. M.; Mirghani, M. E. S.; Saheed, O. K. Are deep eutectic solvents benign or toxic? *Chemosphere* **2013**, *90*, 2193−2195.

(36) van Osch, D. J. G. P.; Zubeir, L. F.; van den Bruinhorst, A.; Rocha, M. A. A.; Kroon, M. C. Hydrophobic deep eutectic solvents as water-immiscible extractants. *Green Chem.* **2015**, *17*, 4518−4521.

(37) Cao, J.; Yang, M.; Cao, F.; Wang, J.; Su, E. Tailor-made hydrophobic deep eutectic solvents for cleaner extraction of polyprenyl acetates from Ginkgo biloba leaves. *J. Clean. Prod.* **2017**, *152*, 399−405.

(38) Ribeiro, B. D.; Florindo, C.; Iff, L. C.; Coelho, M. A. Z.; Marrucho, I. M. Menthol-based eutectic mixtures: hydrophobic low viscosity solvents. *ACS Sustainable Chem. Eng.* **2015**, *3*, 2469−2477.

(39) van Osch, J. C. P.; Parmentier, D.; Dietz, C. H. J. T.; van den Bruinhorst, A.; Tuinier, R.; Kroon, M. C. Removal of alkali and transition metal ions from water with hydrophobic deep eutectic solvents. *Chem. Commun.* **2016**, *52*, 11987−11990.

(40) Ruggeria, S.; Polettia, F.; Zanardia, C.; Pigania, L.; Zanfogninia, B.; Corsi, E.; Dossi, N.; Salomäki, M.; Kivelä, H.; Lukkari, J.; Terzi, F. Chemical and electrochemical properties of a hydrophobic deep eutectic solvent. *Electrochim. Acta* **2019**, *295*, 124−129.

(41) Florindo, C.; Branco, L. C.; Marrucho, I. M. Development of hydrophobic deep eutectic solvents for extraction of pesticides from aqueous environments. *Fluid Phase Equilib.* **2017**, *448*, 135−142.

(42) Jeong, E.; Jung, M. J.; Cho, S.-H.; Lee, S. I.; Lee, Y. S. Surface and electrochemical properties of amino-fluorinated activated carbon. *Colloids Surf. A: Physicochem. Eng. Asp.* **2011**, *377*, 243−250.

(43) Li, Z.; Kim, J. K.; Chaudhari, V.; Mayadevi, S.; Campos, L. C. Degradation of metaldehyde in water by nanoparticle catalysts and powdered activated carbon. *Environ. Sci. Pollut. Res.* **2017**, *24*, 17861−17873.

(44) Zhao, K.; Quan, X.; Chen, S.; Yu, H.; Zhao, J. Preparation of fluorinated activated carbon for electro-Fenton treatment of organic pollutants in coking wastewater: The influences of oxygen containing groups. *Sep. Purif. Technol.* **2019**, *224*, 534−542.

(45) Diyuk, V. E.; Zaderko, A. N.; Grishchenko, L. M.; Afonin, S.; Mariychuk, R.; Kaňuchová, M.; Lisnyak, V. V. Preparation, texture and surface chemistry characterization of nanoporous-activated carbons co-doped with fluorine and chlorine. *Appl. Nanosci.* **2022**, *12*, 2103−2116.

(46) Velasco, L. F.; Kim, K. H.; Lee, Y.-S.; Lodewyckx, P. Influence of fluorine doping of activated carbon fibers on their water vapor adsorption characteristics. *Front. Chem.* **2021**, *8*, No. 593756.

(47) Lee, Y. S. Syntheses and properties of fluorinated carbon materials. *J. Fluor. Chem.* **2007**, *128*, 392−403.

(48) Kim, J.; Chun, J.; Kim, S.-G.; Ahn, H.; Roh, K.-C. Nitrogen and fluorine co-doped activated carbon for supercapacitors. *J. Electrochem. Sci. Technol.* **2017**, *8*, 338−343.

(49) Bard, A.J.; Faulkner, L.R.*Electrochemical Methods: Fundamentals and Applicationds*, 2nd Ed.; Wiley: New Jersey, 2000.

(50) Arab, N.; Fotouhi, L.; Salis, A.; Dorraji, P. S. An amplified electrochemical sensor employing a polymeric film and graphene quantum dots/multiwall carbon nanotubes in a deep eutectic solvent for sensitive analysis of paracetamol and 4-aminophenol. *New J. Chem.* **2020**, *44*, 15742−15751.

(51) Jung, M.-J.; Jeong, E.; Kim, S.; Lee, S. I.; Yoo, J.-S.; Lee, Y.-S. Fluorination effect of activated carbon electrodes on the electrochemical performance of electric double layer capacitors. *J. Fluor. Chem.* **2011**, *132*, 1127−1133.

(52) Weerasooriyagedara, M.; Ashiqa, A.; Gunatilake, S. R.; Giannakoudakis, D. A.; Vithanage, M.Surface interactions of oxytetracycline on municipal solid waste-derived biochar-montmorillonite composite. *Sustain. Environ.***2022**, *8*, DOI: 10.1080/27658511.2022.2046324.

(53) Ries, M. A. E.; Wassel, A. A.; Ghani, N. T. A.; El-shall, M. A. Electrochemical adsorptive behavior of some fluoroquinolones at carbon paste electrode. *Anal. Sci.* **2005**, *21*, 1249−1254.

(54) Laviron, E. General expression of the linear potential sweep voltammogram in the case of diffusionless electrochemical systems. *J. Electroanal. Chem. Interfacial Electrochem.* **1979**, *101*, 19−28.

(55) Leal, J. F.; Santos, E. B. H.; Esteves, V. I. Oxytetracycline in intensive aquaculture: water quality during and after its administration, environmental fate, toxicity and bacterial resistance. *Rev. Aquacult.* **2019**, *11*, 1176−1194.

(56) Magesa, F.; Wu, Y.; Dong, S.; Tian, Y.; Li, G.; Vianney, J. M.; Buza, J.; Liu, J.; He, Q. Electrochemical sensing fabricated with Ta_2O_5 nanoparticle-electrochemically reduced graphene oxide nanocomposite for the detection of oxytetracycline. *Biomolecules* **2020**, *10*, 110.

(57) Florindo, C.; Lima, F.; Branco, L. C.; Marrucho, I. M. Hydrophobic Deep Eutectic Solvents: A Circular Approach to Purify Water Contaminated with Ciprofloxacin. *ACS Sustainable Chem. Eng.* **2019**, *7*, 14739−14746.

(58) Rabboh, F. M.; Neil, G. D. O. Voltammetric pH measurements in unadulterated foodstuffs, urine, and serum with 3d-printed graphene/poly(lactic acid) electrodes. *Anal. Chem.* **2020**, *92*, 14999−15006.

(59) Ajami, N.; Panah, N. B.; Danaee, I. Oxytetracycline nanosensor based on poly-ortho aminophenol/multi-walled carbon nanotubes composite film. *Iran. Polym. J.* **2014**, *23*, 121−126.

(60) Sun, J.; Gan, T.; Zhu, H.; Shi, Z.; Liu, Z. Y. Direct electrochemical sensing for oxytetracycline in food using a zinc cation-exchanged montmorillonite. *Appl. Clay Sci.* **2014**, *101*, 598−603.

(61) Sun, J.; Chang, L.; Li, H.; Liu, Y. Electrochemical determination of oxytetracycline in animal-derived food based on Cu_2O microspheres modified electrode. *J. Xinyang Normal Univ. Nat. Sci. Ed.* **2019**, *32*, 126−131.